Research article

Dmitry A. Chermoshentsev, Evgeny V. Anikin, Sergey A. Dyakov* and Nikolay A. Gippius

Dimensional confinement and waveguide effect of Dyakonov surface waves in twisted confined media

https://doi.org/10.1515/nanoph-2020-0459
Received August 6, 2020; accepted September 28, 2020;
published online October 26, 2020

Abstract: We theoretically study Dyakonov surface waveguide modes that propagate along the planar strip interfacial waveguide between two uniaxial dielectrics. We demonstrate that owing to the one-dimensional electromagnetic confinement, Dyakonov surface waveguide modes can propagate in the directions that are forbidden for the classical Dyakonov surface waves at the infinite interface. We show that this situation is similar to a waveguide effect and formulate the resonance conditions at which Dyakonov surface waveguide modes exist. We demonstrate that the propagation of such modes without losses is possible. We also consider a case of two-dimensional confinement, where the interface between two anisotropic dielectrics is bounded in both orthogonal directions. We show that such a structure supports Dyakonov surface cavity modes. Analytical results are confirmed by comparing with full-wave solutions of Maxwell's equations. We believe that our work paves the way toward new insights in the field of surface waves in anisotropic media.

Keywords: anisotropic materials; Dyakonov surface waves; electromagnetic confinement; optical cavity; surface waves; waveguide.

***Corresponding author: Sergey A. Dyakov**, Skolkovo Institute of Science and Technology, Moscow Region, Russia,
E-mail: s.dyakov@skoltech.ru. https://orcid.org/0000-0002-3729-6621
Dmitry A. Chermoshentsev, Skolkovo Institute of Science and Technology, Moscow Region, Russia; Moscow Institute of Physics and Technology, Moscow Region, Russia; and Russian Quantum Center, Moscow Region, Russia, E-mail: dmitry.chermoshentsev@skoltech.ru. https://orcid.org/0000-0002-4140-4947
Evgeny V. Anikin and Nikolay A. Gippius, Skolkovo Institute of Science and Technology, Moscow Region, Russia,
E-mail: Evgenii.Anikin@skoltech.ru (E.V. Anikin), n.gippius@skoltech.ru (N.A. Gippius). https://orcid.org/0000-0002-2966-3735 (E.V. Anikin)

1 Introduction

Surface electromagnetic waves, propagating along the interface of two dissimilar media, have been the subject of extensive research during the last decades as they represent one of the fundamental concepts of nanophotonics. Understanding the optical properties of surface waves is of great importance for realizing their practical application.

There are several types of surface waves that differ in material type, domain of existence, propagation constant, decay profile. Among different types of surface waves, there are surface plasmon-polariton at a metal-dielectric interface [1], Tamm surface states at a photonic crystal boundary [2–4], surface solitons at a nonlinear interface [5], and many others.

Another family of surface waves is Dyakonov surface waves (DSWs), which exist at the interface of two media at least one of which is anisotropic, as predicted in 1988 in the study by D'yakonov [6]. In this pioneering work, the first medium was considered as an isotropic dielectric with the refractive index n_m, whereas the second medium was an anisotropic uniaxial dielectric with the refractive indices n_o and n_e and an optical axis is parallel to the interface. It has been shown that DSWs exist in such a system if the condition

$$n_o < n_m < n_e \tag{1}$$

is satisfied. In 1998, Walker et al. extended the theory of DSWs to the case of biaxial medium [7] with refractive indices $n_x < n_y < n_z$. In isotropic/biaxial system, the condition (1) transforms into

$$n_x < n_y < n_m < n_z. \tag{2}$$

Later, different combinations of isotropic, uniaxial, biaxial, and chiral materials have been demonstrated to support DSWs [8–14].

A narrow range of propagation angles makes the experimental observation of DSWs rather complicated [15]. As a result, the first detection of these waves has been demonstrated only in 2009 [16]. The authors used Otto-Kretschmann configuration to observe Dyakonov

surface states at the interface of a biaxial crystal and an isotropic liquid. Another perspective approach to obtain Dyakonov-like surface waves experimentally is the usage of partnering thin films between anisotropic and isotropic media [17]. In such systems, the direction of hybrid Dyakonov-guided modes propagation can be controlled by changing the isotropic medium's refractive index. The results presented in the study by Takayama, Artigas, and Torner [17] show that these types of waves can be used as a sensing unit. It has been demonstrated in a number of publications that DSWs can exist at the interface of isotropic materials and materials with artificially designed shape anisotropy [9, 18–22]. Moreover, as theoretically shown in Ref. [23, 24], in the metamaterial composed of alternating layers of metals and dielectric, exotic types of surface waves such as Dyakonov plasmons and hybrid plasmons can appear. In such structures, the angular range of existence of DSWs can be extended up to $\Delta\phi \sim 65°$.

Recently, in 2019, a new type of surface waves, referred to as Dyakonov-Voigt surface waves, have been theoretically demonstrated at the interface of isotropic and uniaxial materials [25]. Unlike conventional DSWs, Dyakonov-Voigt surface waves decay is the product of a linear and an exponential function of the distance from the interface in anisotropic medium [26–28]. In contrast to DSWs, Dyakonov-Voigt surface waves propagate only in one direction in each quadrant of the interface plane.

Like in the cases of other surface waves, the feasibility of the practical use of DSWs ultimately depends on whether they can exist in resonator structures of finite size and whether they can propagate without radiative losses. In Ref. [29], it has been shown that the DSWs can be conformally transformed into the bound states of cylindrical metamaterials. Dyakonov-like surface waves have been also theoretically predicted in anisotropic cylindrical waveguides [30]. Owing to the bending of the waveguide boundary, such modes have inevitable radiative losses. In our recent work [44] we considered Dyakonov-like waveguide modes in a flat interfacial strip waveguide confined in the dimension perpendicular to the DSW propagation direction and showed that such modes can propagate without radiative losses.

This article is devoted to the theoretical study of Dyakonov-like surface states at a flat interface confined in one or two dimensions. Like in Ref. [44], we consider two anisotropic uniaxial lossless dielectrics twisted in such a way that their optical axes form an angle of 90° to each other and are parallel to the interface between dielectrics. In contrast to Ref. [44], here such a system is confined in the dimensions parallel or perpendicular to the optical axes. We study Dyakonov surface waveguide modes (DSWM) in the case of one-dimensional electromagnetic confinement and show that the propagation of such modes without radiative losses is possible. We also introduce the concept of Dyakonov surface cavity modes in the case of two-dimensional confinement.

2 Interface of two uniaxial crystals

We start our discussion by considering a flat infinite interface between two twisted semi-infinite anisotropic uniaxial media shown in Figure 1a. We assume that the optical axes of the upper and lower media are directed along the x and y coordinate axes. As shown in Refs. [31–33], such a configuration supports DSWs when anisotropic media are optically positive, that is, the condition (1) is satisfied. In Refs. [34–37], the problem of DSWs has been generalized to the case of two biaxial crystals. In this section, we once again describe some of the key points of DSWs in the uniaxial/uniaxial configuration which are crucial for understanding the properties of Dyakonov-like surface waves in confined media. We denote the dielectric permittivity tensor of the upper half-space as $\hat{\varepsilon}_{\text{up}} = \text{diag}(\varepsilon_2, \varepsilon_1, \varepsilon_1)$ and of the lower half-space as $\hat{\varepsilon}_{\text{low}} = \text{diag}(\varepsilon_1, \varepsilon_2, \varepsilon_1)$. DSWs in such a system can be obtained as a linear combination of exponentially decaying ordinary and extraordinary waves which are solutions of Maxwell's equation in each half-space:

$$\left.\begin{aligned} \vec{E}^{+}_{\text{DSW}} &= C^{+}_{o}\vec{E}^{+}_{o} + C^{+}_{e}\vec{E}^{+}_{e} \\ \vec{B}^{+}_{\text{DSW}} &= C^{+}_{o}\vec{B}^{+}_{o} + C^{+}_{e}\vec{B}^{+}_{e} \end{aligned}\right\} \quad \text{at} \quad z > 0, \\ \left.\begin{aligned} \vec{E}^{-}_{\text{DSW}} &= C^{-}_{o}\vec{E}^{-}_{o} + C^{-}_{e}\vec{E}^{-}_{e} \\ \vec{B}^{-}_{\text{DSW}} &= C^{-}_{o}\vec{B}^{-}_{o} + C^{-}_{e}\vec{B}^{-}_{e} \end{aligned}\right\} \quad \text{at} \quad z < 0. \tag{3}$$

where $\vec{E}$ and $\vec{B}$ are the electric and magnetic vectors, $C^{\pm}_{o}$ and $C^{\pm}_{e}$ are the coefficients of the linear combination and signs "+" and "−" denote upper and lower half-spaces, respectively. Using the expressions for ordinary and extraordinary waves in upper and lower anisotropic media (see Supplemental Materials) and taking into account the continuity of the in-plane field components at the interface, after algebraic manipulations, one can obtain the dispersion relation of DSWs in the following form

$$\det\begin{pmatrix} 0 & k_0^2\varepsilon_1 - k_x^2 & k_0 k_z^{o-} & k_x k_y \\ k_0^2\varepsilon_1 - k_x^2 & 0 & k_x k_y & -\varepsilon_1 k_0 k_z^{e-} \\ -k_0 k_z^{o+} & k_x k_y & 0 & k_0^2\varepsilon_1 - k_y^2 \\ k_x k_y & \varepsilon_1 k_0 k_z^{e+} & k_0^2\varepsilon_1 - k_y^2 & 0 \end{pmatrix} = 0 \tag{4}$$

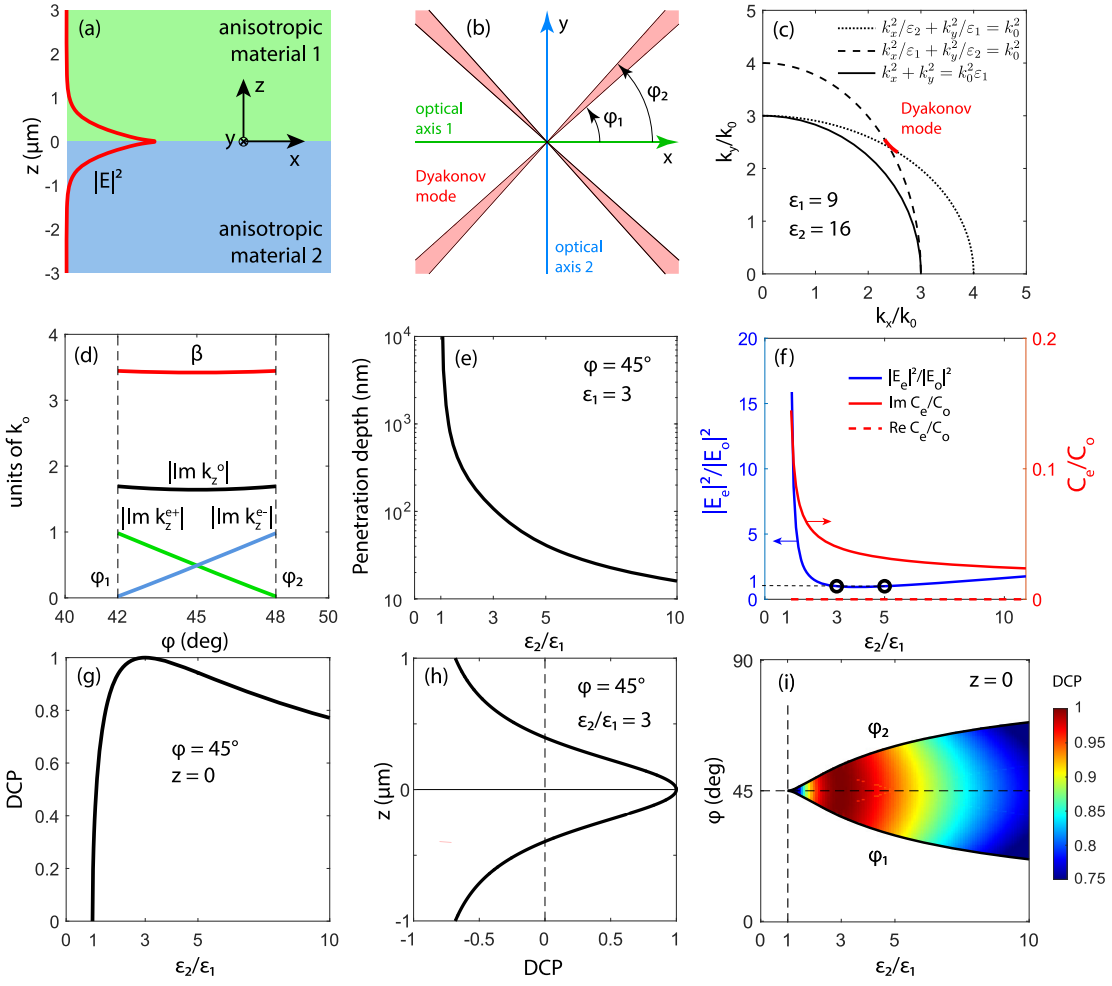

Figure 1: (Color online) (a) The interface between two anisotropic materials. Red lines show the profile of electric field intensity. (b) Top view of the interface. Red shaded regions show the propagation cones of DSWs. Angles φ_1 and φ_2 are the limits of the φ-range of the existence of DSWs. (c) Ordinary wave (solid black line) and extraordinary waves in anisotropic materials 1 and 2 (dashed and dotted lines) as well as DSW (red line) in reciprocal space. (d) Azimuthal angle dependencies of propagation constant β of DSW and the absolute value of imaginary parts of z-projections of wavevectors of ordinary and extraordinary waves in anisotropic materials 1 and 2 with $\varepsilon_1 = 9$ and $\varepsilon_2 = 16$. Black dashed lines bound the φ-range of the existence of DSWs. (e) The penetration depth of DSW into upper and lower anisotropic media at $\varphi = 45°$. (f) The ratio of electric field intensities of ordinary and extraordinary waves which form DSW (blue line) and the ratio of coefficients C_e/C_o (red lines) as functions of anisotropy factor $\gamma = \varepsilon_2/\varepsilon_1$. (g) Degree of circular polarization (DCP) of DSW at $z = 0$ propagating at $\varphi = 45°$ as a function of anisotropy factor γ. (h) DCP of DSW propagating at $\varphi = 45°$ as a function of coordinate z at $\varepsilon_2/\varepsilon_1 = 3$. (i) Thick black lines denote the limits of the φ-range existence of DSWs as functions of anisotropy factor, $\varphi_2(\varepsilon_2/\varepsilon_1)$ and $\varphi_1(\varepsilon_2/\varepsilon_1)$. Colormap shows the anisotropy factor and azimuthal angle dependence of the DCP of DSW. Colorscale is shown on the right. DSW, Dyakonov surface wave.

where $k_0 = 2\pi/\lambda$ is the vacuum wavenumber, k_x, k_y, and k_z are the wavevector components, λ is the wavelength and the z-components of wavevectors are:

$$\left.\begin{aligned} k_z^{o+} &= \sqrt{k_0^2\varepsilon_1 - k_x^2 - k_y^2}, \\ k_z^{e+} &= \sqrt{k_0^2\varepsilon_2 - \gamma k_x^2 - k_y^2}, \end{aligned}\right\} \text{ at } z > 0, \qquad \left.\begin{aligned} k_z^{o-} &= -\sqrt{k_0^2\varepsilon_1 - k_x^2 - k_y^2} \\ k_z^{e-} &= -\sqrt{k_0^2\varepsilon_2 - k_x^2 - \gamma k_y^2} \end{aligned}\right\} \text{ at } z > 0. \tag{5}$$

where $\gamma = \varepsilon_2/\varepsilon_1$ is the anisotropy factor. In Eq. (5), all k_z are purely imaginary and the signs of square roots are chosen in such a way that the solution decays with distance from the interface in upper and lower half-spaces.

The numerical solution of the Equation (4) for the Dyakonov wave is represented in Figure 1c by the red curve. One can see that the DSW is located near the intersection of the dispersion curves of extraordinary waves with $k_z = 0$ in the upper and lower half-spaces. The (k_x, k_y) range of the existence of DSW determines the narrow domain of azimuthal angle φ near the bisector

between the crystals' optical axes where the DSW can propagate (Figure 1b). This is in agreement with the results reported in Refs. [31, 33, 38] for the two symmetrical uniaxial anisotropic crystals.

The φ –angular dependencies of $\left|\mathrm{Im}\left(k_z^{o,e}\right)\right|$ and the propagation constant $\beta(\varphi) = \sqrt{k_x^2 + k_y^2}$ for permittivities $\varepsilon_1 = 9$ and $\varepsilon_2 = 16$ are presented in Figure 1d. One can see that the extraordinary wave decays slower than the ordinary wave. In the cutoff points φ_1 and φ_2, the imaginary part of $\left|\mathrm{Im}\left(k_z^{e}\right)\right|$ turns to zero and the solution is no longer localized near the interface. It is worth noting that at $\varphi = 45°$, the absolute values of k_z^{e+} and k_z^{e-} are the same, and the DSW decays to the upper and lower half-spaces equally.

To estimate the partial contributions of ordinary and extraordinary waves to the DSW, we calculate the ratio of the coefficients C_e/C_o, as well as the ratio of the electric field intensities $|E_e|^2/|E_o|^2$ in the most symmetric case $\varphi = 45°$ when $C_{o,e}^{+} = C_{o,e}^{-}$ and $\left|E_{o,e}^{+}\right|^2 = \left|E_{o,e}^{-}\right|^2$. Figure 1f demonstrates that at $\gamma \lesssim 2$, the contribution of the extraordinary wave is dominant. Knowledge of the partial contributions of the ordinary and extraordinary waves to the DSW and their decay constants $\mathrm{Im}k_z$ (Figure 1d) enables us to find the resulting penetration depth of DSW into the upper and lower anisotropic dielectrics (Figure 1e). One can see in Figure 1e that with the increase of the anisotropy factor, the DSW becomes more localized at the interface.

The dispersion relation of DSW can be found analytically from Eq. (4) for the symmetric case of $\varphi = 45°$ ($k_x = k_y$), when the DSW propagates along the bisector. The expression for the propagation constant of DSW in this case reads:

$$\beta(\pi/4) = k_0\sqrt{\frac{\varepsilon_1 + \sqrt{(2\varepsilon_2 - \varepsilon_1)\varepsilon_1}}{2}}. \tag{6}$$

Moreover, Eq. (4) can also be analytically solved in the cutoff points φ_1 and φ_2 of the angular domain of existence. At $\varphi = \varphi_1$ we get

$$k_x(\varphi_1) = k_0\sqrt{\varepsilon_1}\sqrt{\frac{\gamma(\gamma+2) - \sqrt{\gamma(\gamma^2+\gamma-1)}}{2(\gamma+1)}}, \tag{7}$$

$$k_y(\varphi_1) = k_0\sqrt{\varepsilon_1}\sqrt{\frac{\gamma^2 + \sqrt{\gamma(\gamma^2+\gamma-1)}}{2\gamma(\gamma+1)}}. \tag{8}$$

This gives us the analytical expression for the cutoff angle φ_1:

$$\tan\varphi_1 = \frac{k_y(\varphi_1)}{k_x(\varphi_1)} = \sqrt{\frac{\gamma^2 + \sqrt{\gamma(\gamma^2+\gamma-1)}}{\gamma^2(\gamma+2) - \gamma\sqrt{\gamma(\gamma^2+\gamma-1)}}}. \tag{9}$$

Owing to the symmetry, the second cutoff angle φ_2 can be determined by swapping k_x and k_y. This brings us to a simple relation $\tan\varphi_2 = \cot\varphi_1$ (Figure 1b). One can see from Eq. (9) that the cutoff angles depend only on the anisotropy factor $\gamma = \varepsilon_2/\varepsilon_1$ and does not depend on the values of ε_1 and ε_2. We also notice that the higher the anisotropy factor, the larger the angular domain of existence (Figure 1i). Owing to the structure symmetry, the DSW can propagate in identical angular domains rotated relative to the OZ axis by $\pi/2$ (Figure1b).

Like many surface waves, DSWs are elliptically polarized. However, the degree of circular polarization (DCP) depends on the anisotropy factor γ, on the azimuthal angle of propagation φ and on the coordinate z where the electric field is considered. For the most symmetric case ($\varphi = 45°$, $z = 0$) the γ-dependence of the DCP can be expressed analytically:

$$\mathrm{DCP} = 2\sqrt{2}\ \frac{\sqrt{\gamma-1}}{\gamma+1}. \tag{10}$$

From Eq. (10), we can see that at $\gamma = 3$, the DCP equals to 1 (Figure 1g) which corresponds to a purely circularly polarized field. In the limit of a low anisotropy, the DCP goes to 0 and the DSW becomes almost linearly polarized. By means of full-wave electromagnetic simulations made by scattering matrix method [39–41], we calculate the DCP in a less symmetric case when $z \neq 0$. We obtain that with distance from the interface, the orientation of polarization cones in DSW changes, wherein the DCP decreases and changes its sign (Figure 1h). We also vary the azimuthal angle φ (Figure 1i) and find that the φ-dependence of the DCP is weak, however for all $\varphi \neq 45°$ DCP < 1.

3 Reflection from boundary

Before moving on to exploring the dimensional confinement of Dyakonov-like surface states, it is important to analyze the scattering of a DSW on a single boundary perpendicular to the interface plane along which the DSW propagates. The results obtained in the previous section provide the possibility for performing this analysis.

We consider a DSW propagating along the interface at a varying azimuthal propagation angle φ and hitting the boundary at a varying angle of incidence α (Figure 2a). In this section, we use a new coordinate system where the boundary is parallel to the y-axis and the angle between the optical axes and coordinate axes equals to $\varphi - \alpha$. We consider two cases when the boundary separates anisotropic materials from (i) air and (ii) perfect electric conductor (PEC). In reflection, the y-component of the wavevector $k_y(\alpha)$ is conserved and, hence, can be

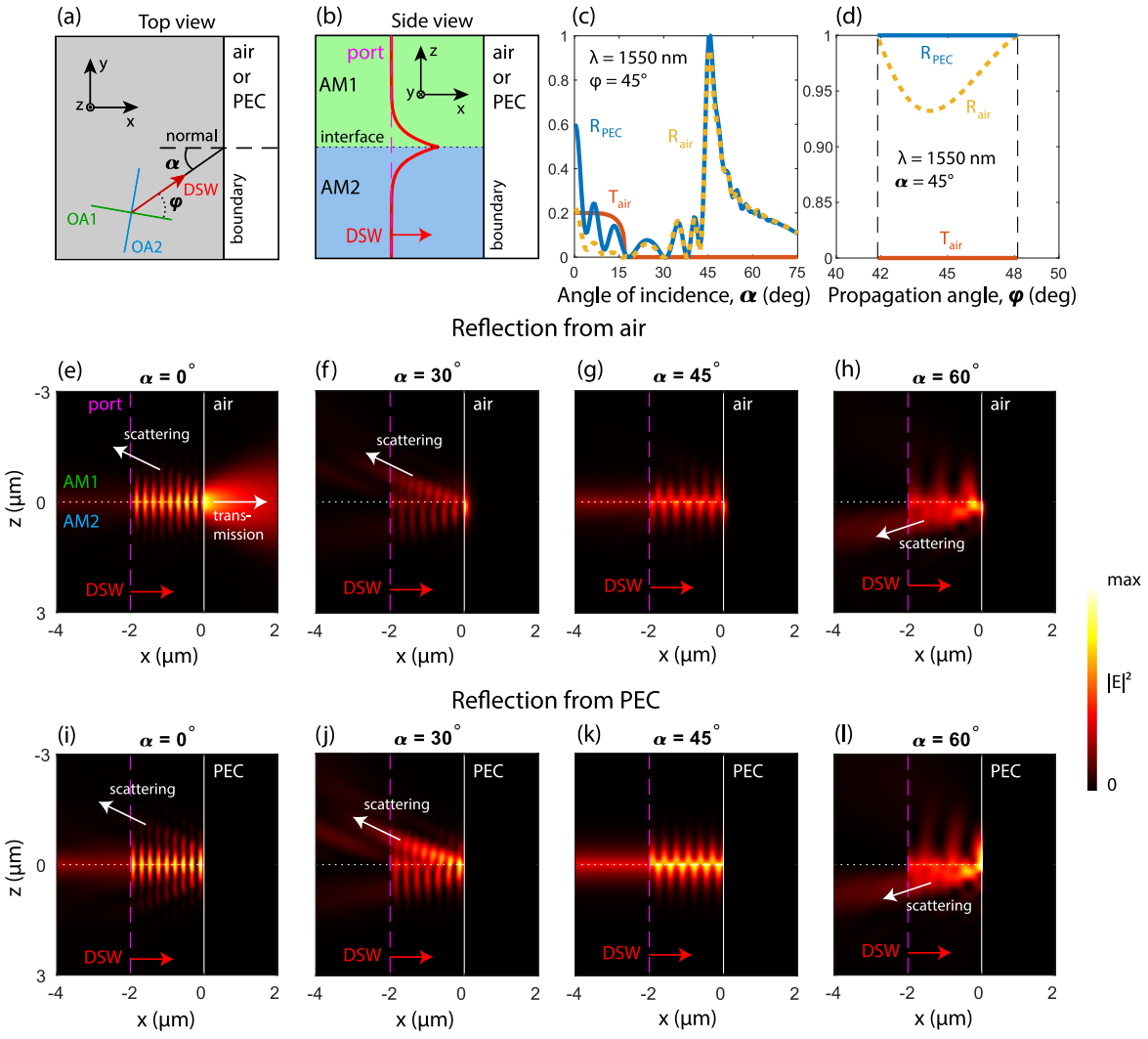

Figure 2: (Color online) Top view (a) and side view (b) of the interface between two anisotropic materials bounded by air or a perfect electric conductor (PEC) half-space on the right. In panel b, the red line schematically shows the Dyakonov surface wave, which is induced by the port denoted by the dashed magenta line, and then hits the boundary. (c and d) The α- and φ-angular dependencies of specular reflection and transmission in such a configuration. In d, the black dashed lines bound the φ-range of the existence of Dyakonov surface waves (DSWs) in the infinite interface. Vertical cross-section of electric field intensity when DSW hits the air boundary (e–h) or the PEC boundary (i–l) calculated at different incident angles α. Arrows show the direction of scattering and transmission. All simulations are made for $\lambda = 1550$ nm, $\varepsilon_1 = 9$ and $\varepsilon_2 = 16$. Colorscale is shown on the right.

described by the propagation constant β in the following way:

$$k_y(\alpha, \varphi) = \beta(\varphi) \sin(\alpha + \varphi - \pi/4). \quad (11)$$

It enables us to reduce the 3D scattering problem to a 2D problem in the XZ plane with a fixed out-of-plane wavevector component $k_y(\alpha, \varphi)$ and the corresponding orientation of optical axes of anisotropic materials (Figure 2b). We perform the corresponding electromagnetic simulations of DSW scattering on the boundary using the finite element method in COMSOL Multiphysics.

First, we explore the most symmetric configuration fixing the azimuthal propagation angle at $\varphi = 45°$ and calculate the specular reflection and transmission coefficients at varying α for the air or PEC boundaries (Figure 2c). Because both the incident and the reflected DSWs can only propagate in the limited domain near the bisector between the optical axes, the reflection of this mode without significant scattering losses can occur only at the angle α close to 45°. In the case of air boundary, the transmission turns to zero at $\alpha > 17.5°$ which is due to the total internal reflection at incident angles exceeding

the critical angle. Please note that we do not consider the transmission to PEC because it is zero by definition.

Second, we consider the case of the maximal reflection by fixing the incident angle α at 45° and varying the azimuthal propagation angle φ within the φ-range of DSW existence $[\varphi_1, \varphi_2]$ (Figure 2d). Please, note that in the considered case, the crystals' orientation is fixed. One can see in Figure 2d that for the PEC boundary, the reflectance of DSW is independent of φ and equals to 1. In the case of the air boundary, the reflection coefficient $R < 1$ for all φ except for the cutoff points φ_1 and φ_2, where the DSW transforms into the extraordinary propagating wave of one of the two half-spaces. The asymmetry of the reflection coefficient profile results from i) the nonidentity of the upper and lower half-spaces in the presence of the boundary; ii) asymmetry of the decay profiles of DSW in the upper and lower half-spaces at $\varphi \neq 45°$ (see Figure 1d).

Figure 2e–l shows the profiles of the period average electric field intensity of the DSW being produced by the port and falling on the boundary at different incident angles α and at a fixed azimuthal propagation angle $\varphi = 45°$. One can see from Figure 2e that at $\alpha = 0°$, the incident wave is partially reflected, scattered, and transmitted to the air. Intensity modulation between the port and the boundary is due to the interference of the incident and the reflected DSWs. At $\alpha = 45°$ (Figure 2g), the DSW is reflected back to the interface. In the case of the air boundary, there is a slight scattering that occurs only to the incident side as there is a total internal reflection. The specularly reflected DSW propagates perpendicularly to the incident DSW, along the second bisector between two orthogonal optical axes. In the less symmetric cases of $\alpha = 30°$ and 60°, the wave is scattered out to the anisotropic media almost completely. Similar behavior of DSW is observed for the case of PEC boundary with the exception of the fact that at $\alpha = 45°$ no scattering occurs.

We would like to emphasize once again that a non-perfect reflection at $\alpha = 45°$ from the air boundary occurs due to the coupling of DSW to the propagating modes of the upper and lower half-spaces, but not due to the transmission to the air.

4 One-dimensional confinement

Let us now study the system of upper and lower slabs, tangent to each other, confined between two parallel boundaries located at $x = 0$ and $x = d$ as shown in Figure 3a and b. Like in the previous section, we consider the cases of air or PEC boundaries. In Figure 2, we have demonstrated that the maximal reflectance of DSW from the boundary is reached at the incident angle $\alpha = 45°$. If the reflected wave encounters yet another boundary, parallel to the first one, then the process of multireflection continues and lasts until the energy is lost because of scattering. Provided that one of the optical axes is parallel to the boundary while another one is perpendicular to the boundary (Figure 3b), one can expect the existence of a DSWM in the system of two anisotropic materials confined between two boundaries. While one can also consider the case of $\alpha = 0$ where the refection spectrum in Figure 2c has a local maximum (see Supplemental Materials for details), in this section we focused on $\alpha = 45°$.

Because such a strip waveguide has mirror symmetries $x \to -x$ and $y \to -y$, in the case of ideal reflection by PEC, it is possible to treat the propagation of DSWM analytically quite easily. If a solution for DSWs in the infinite interface

$$\vec{E}_{k_x,k_y}(x,y,z) = \vec{E}_{k_x,k_y}(z)e^{ik_x x + ik_y y} \tag{12}$$

is known then the solution for DSWMs which satisfies mirror boundary conditions at $x = 0$ is the following:

$$\overrightarrow{E^{\text{tot}}}(x,y,z) = \vec{E}_{k_x,k_y}(z)e^{ik_x x + ik_y y} - \vec{E}_{-k_x,k_y}(z)e^{-ik_x x + ik_y y}. \tag{13}$$

Moreover, it also satisfies mirror boundary conditions at $x = d$ provided that $k_x d = \pi n$, where $n \in \mathbb{N}$.

These considerations enable us to find the dispersion law of DSWMs. First, we note that the dispersion law of DSW at an infinite interface in xy-plane can be written in a form

$$F\left(\frac{k_x}{k_0}, \frac{k_y}{k_0}\right) = 0, \tag{14}$$

where a function F does not depend on k_0 explicitly (see Eq. (4)). From the condition $k_x d = \pi n$, the dispersion relation of the DSWM propagating along the y-axis with the propagation constant k_y has the following form:

$$F\left(\frac{\pi n}{k_0 d}, \frac{k_y}{k_0}\right) = 0\,, \tag{15}$$

where n is the mode order.

The dispersion curves of DSWMs $k_0(k_y)$ calculated by Eq. (15) for the case of the PEC boundary and by COMSOL for the case of air boundary are shown in Figure 3c and g by black and red lines, respectively. For comparison, Figure 3c and g also show the dispersions of extraordinary waveguide modes (EWMs) of the upper and lower slabs, which are, respectively, TE and TM polarized because of the specific dielectric tensor orientations

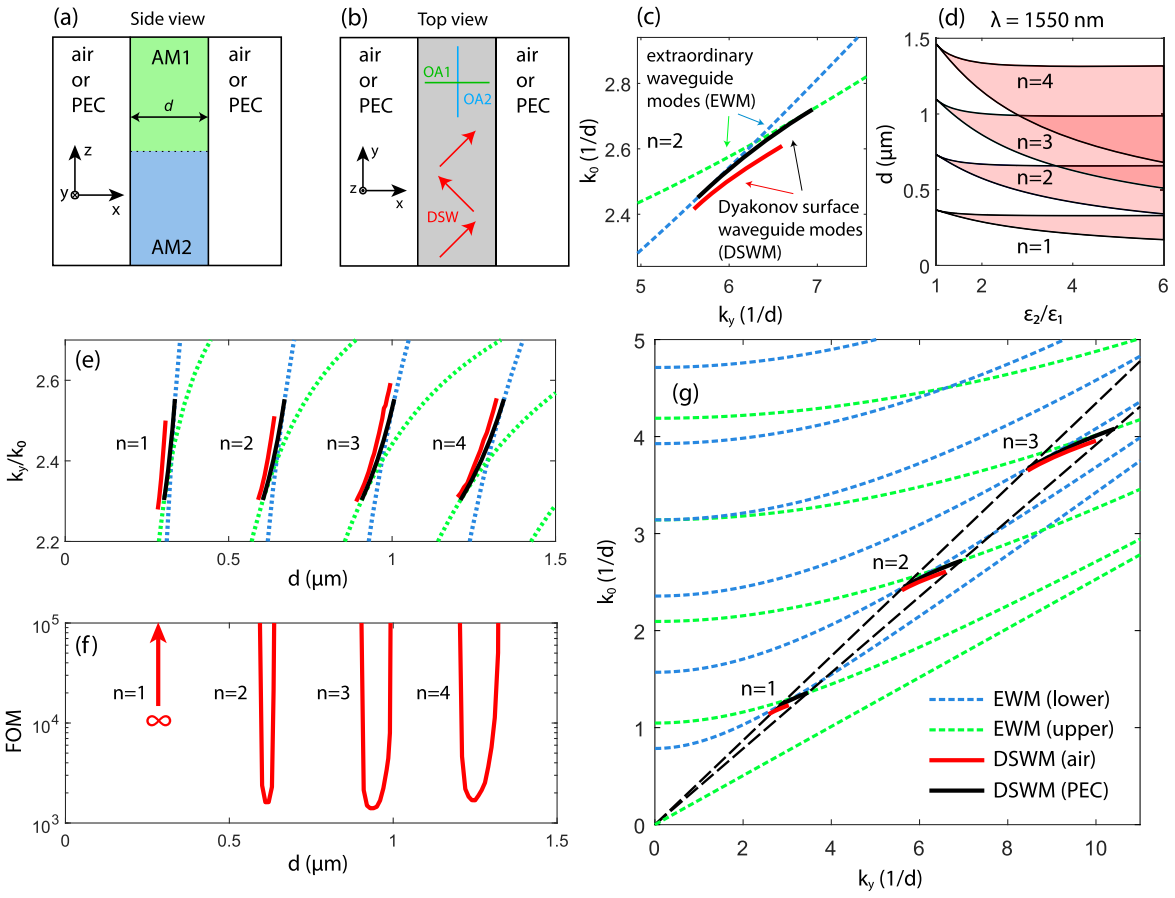

Figure 3: (Color online) Side view (a) and top view (b) of the interface between two anisotropic materials bounded by air or PEC half-spaces from left and right. Optical axes of anisotropic materials are parallel to coordinate axes as shown by the green and blue lines in panel (b). DSWM in such configuration is a superposition of DSWs reflecting from both sides of the boundary at an angle α close to 45° as is shown in panel (b) by red arrows. (c), (e) and (g): Extraordinary waveguide modes (EWM) of the upper and lower anisotropic slabs (dashed green and blue lines) with PEC boundaries and DSWMs in the case of a PEC (solid black line) or air (solid red line) boundary. (d): Range of the waveguide width, d, in which DSWMs exist. (f): Figure of merit (FOM) calculated for the case of air boundary. All calculations are made for $\varepsilon_1 = 9$, $\varepsilon_2 = 16$ except for panel (d). PEC, perfect electric conductor; DSW, Dyakonov surface wave; DSWM, Dyakonov surface waveguide mode.

and PEC boundary condition. Both k_y and k_0 are plotted in $1/d$ units, making the displayed dispersion curves universal in terms of the waveguide width d. One can see that the DSWMs appear near the intersection of the EWMs. We note that the dispersion curves of DSWMs have the cutoff points which originate from the angular cutoffs[1] φ_1 and φ_2 of the DSWs at the infinite interface. Each point on the dispersion curves between the cutoffs corresponds to a certain azimuthal propagation angle φ. Please note that because the orientation of optical axes of the upper and lower waveguides is fixed, the angle φ ultimately determines the angle of incidence α. Hence, each point on the DSWM dispersion curves also corresponds to a certain angle of incidence α close to 45°.

The waveguide width dependence of the propagation constant $k_y(d)$ can also be calculated by Eq. (15) for the case of PEC and is shown in Figure 3e along with the same dependence calculated in COMSOL for the case of air. For comparison, $k_y(d)$ dependencies of EWMs of the upper and lower slabs are also shown in Figure 3e. The d-range where DSWM can propagate is determined by the angular existence domain of the DSW at the infinite interface. With an increase of the anisotropy factor, the existence range of DSWM broadens (Figure 3d) and, at large anisotropy, the existence ranges of DSWMs with different mode numbers n overlap. It is worthy to note that we compared the analytical results obtained from Eq. (15) for PEC with full-wave simulations made in COMSOL Multiphysics and observed excellent agreement (not shown in Figure 3).

1 Please note that the cutoff points for DSWM for the air boundary are determined approximately due to limitation of the computational domain size in COMSOL.

As it has been demonstrated in Figure 2, the reflection of DSWMs from the PEC half-space at $\alpha = 45°$ is ideal, meaning that there is no scattering and, therefore, the DSWMs between PEC boundaries are lossless. However, in the case of the air half-space, even at $\alpha = 45°$, the reflection coefficient $R < 1$. This means that in the strip waveguide surrounded by air, DSWMs can have radiative losses that scatter out the DSWM energy to the waveguide modes of the upper and lower slabs. Like in Ref. [30], to describe the radiation losses quantitatively, we calculate the following figure of merit (FOM).

$$\mathrm{FOM} = \frac{\mathrm{Re}\, k_y}{\mathrm{Im}\, k_y}, \tag{16}$$

which has the meaning of a DSWM decay length expressed in units of the DSWM wavelength. Figure 3f shows the FOM calculated in COMSOL. One can see that for $n = 2, 3, 4$, the FOM tends to infinity near the cutoff points while having a local minimum between them. This behavior of the FOM is explained by the DSW reflection profile shown in Figure 2d. Indeed, at the cutoff points, the DSW transforms into the EWMs which have no radiative losses when reflecting from the air boundary. We also observe that for the first-order DSWM ($n = 1$), the FOM is infinite. To explain this remarkable fact, we compare the field symmetries of the DSWMs and the waveguide modes of the upper and lower slabs (see Supplemental Materials).

Our field simulations reveal that for the first-order DSWM, there is the symmetry mismatch and the corresponding overlap integrals vanish, which indicates that the coupling of the first-order DSWM with the slabs' waveguide modes is not possible. As there is also no radiative leakage to the air (see Figure 2f and its discussion), we conclude that the first-order DSWM has no radiative losses which results in the infinite FOM. Radiative losses of higher-order DSWM's are fully attributed to the coupling with the slabs' waveguide modes. We emphasize once again the importance of the obtained result that although DSWMs are generally coupled to propagating EWMs, a symmetry-protected lossless first-order DSWM exists.

Let us consider the field distributions in DSWMs. Cross-sectional electric field profiles of the second-order DSWM in the strip waveguide surrounded by air calculated for different waveguide widths d within the range of the DSWM's existence are shown in Figure 4a. One can see that at $d = 610$ nm, the mode is localized near the interface almost equally penetrating into the upper and lower slabs. While at widths close to the cutoffs, $d = 600$ and 620 nm, the mode localization appears upward- or downward-biased. DSWMs inherit these peculiar properties of their localization from the classical DSWs at the infinite interface. In the case of the PEC boundary, the waveguide widths d_n corresponding to the most symmetric DSWM penetration into the slabs can be found from Eq. (15) by setting the azimuthal propagation angle of DSW as $\varphi = 45°$:

$$d_n = \pi n / k_y. \tag{17}$$

In the case of the air boundary, this condition will be more complex. The biasing of the DSWMs toward upper or lower slabs explains the presence of the local minimum in the waveguide width dependence of the FOM shown in Figure 3f.

Electric and magnetic field intensity profiles of the first-order and the second-order DSWMs are shown in Figure 4b and c for the widths d such that the symmetry condition (17) is satisfied. For the air boundary, the electric field intensity profile of the n-th-order DSWM has $n + 1$ local maxima in the upper slab and n local maxima in the lower slab. Magnetic field intensity has n local maxima in both cases. For the PEC boundary, the situation is different: n (or $n + 1$) local maxima in the upper (or lower) waveguide for the electric field and $n + 1$ local maxima for the magnetic field. Projections of electric and magnetic vectors directions on xz and xy planes are shown in Figure 4d–f for the first-order DSWM. One can see the periodic pattern in Figure 4f which demonstrates the propagation of DSWM along the strip waveguide. It is necessary to note here that electric and magnetic fields in DSWM are elliptically polarized like those in conventional DSWs at the infinite interface; however, the orientation of polarization ellipse and the degree of circular polarization also depend on the x coordinate (see Supplemental Materials for details). The examples of field distribution for cases when $d_n \neq \pi n/k_y$ and for different mode orders n are presented in Supplemental materials.

At the end of this section, we conclude that the one-dimensional electromagnetic confinement makes DSWMs traveling along the direction where classical DSWs cannot propagate. Indeed, as is shown in Figure 1b, DSWs exist at a small angle around the bisector between optical axes of upper and lower anisotropic materials, whereas the DSWMs propagate along one of these optical axes. This feature distinguishes DSWMs from DSWs.

5 Two-dimensional confinement

Owing to the symmetrical configuration of DSWs relative to the optical axes (Figure 1b), one can confine DSWs in two dimensions using two pairs of orthogonal boundaries, as shown in Figure 5a and b. In such a system, the DSW

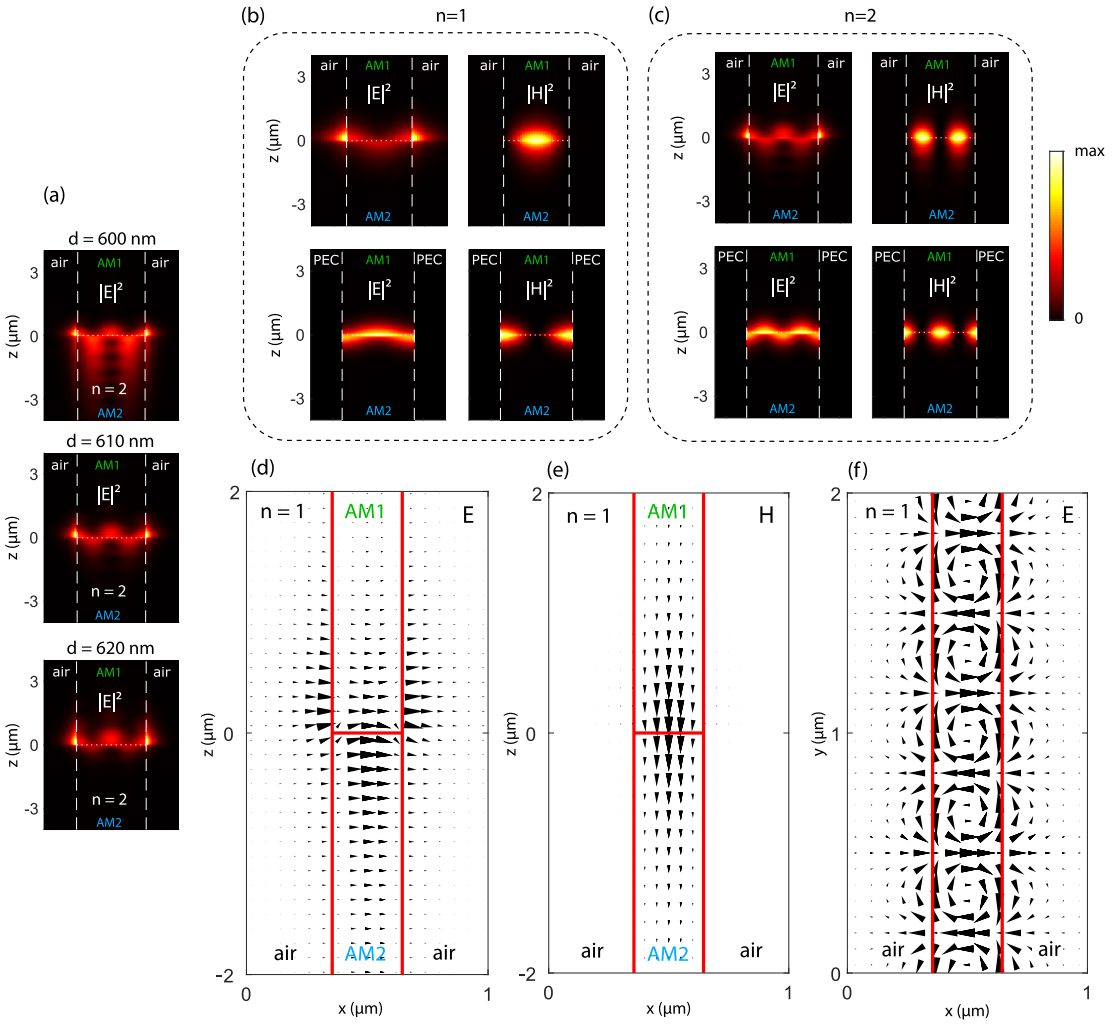

Figure 4: (Color online) (a) Electric field intensity profiles in *xz* cross-section in the second-order DSWM calculated for different waveguide widths. (b, c): Electric field intensity profiles in *xz* cross-section in the first-order and the second-order DSWMs calculated for the air and PEC boundaries. Calculations are made for $d = 290$ nm, $k_y = 9.429\,\mu m^{-1}$ (air, $n = 1$); $d = 320$ nm, $k_y = 9.786\,\mu m^{-1}$ (PEC, $n = 1$); $d = 610$ nm, $k_y = 9.584\,\mu m^{-1}$ (air, $n = 2$); $d = 640$ nm, $k_y = 9.786\,\mu m^{-1}$ (PEC, $n = 2$). Colorscale for panels (a–c) is shown on the right. (d–f) Electric and magnetic vectors in *xz* and *xy* cross-sections. The length of the triangles is proportional to the field strength at the central point of each triangle. Triangles specify the corresponding electric field direction by their orientation. White lines in a–c and red lines in d–f denote the material boundaries. All calculations are made for $\varepsilon_1 = 9$, $\varepsilon_2 = 16$, $\lambda = 1550$ nm. DSWM, Dyakonov surface waveguide mode.

reflects at an angle of $\alpha = 45°$ from four boundaries forming a closed Dyakonov-like surface cavity mode (DSCM), which exists at the interface between two adjacent anisotropic rods of a square cross-section. In such a configuration, optical axes of anisotropic materials have to be parallel to the square's sides. If the rods are surrounded by PEC, then the DSCMs existence condition can be expressed by a simple formula:

$$\beta(\pi/4)d/\sqrt{2} = \pi n, n \in \mathbb{N}, \tag{18}$$

where n is the mode order, d is the side of the square, and $\beta(\pi/4)$ is the propagation constant of the DSW at the infinite interface determined by Eq. (6). Because this condition is only valid for $\alpha = \pi/4$, then, in contrast to one-dimensionally confined DSWMs, DSCMs exist only at a discrete set of the square side d (at a given frequency and dielectric permittivity). The calculated by Eq. (18) values of the square side supporting DSCM are shown in Figure 5c as a function of the anisotropy factor for mode orders $n = 1$–5 and PEC boundaries. These theoretical dependencies are confirmed by full-wave simulations in COMSOL Multiphysics. One can also obtain similar curves for the air boundaries.

We note that the structure with anisotropic rods shown in Figure 5a and b is S_4-symmetrical, that is, it is invariant

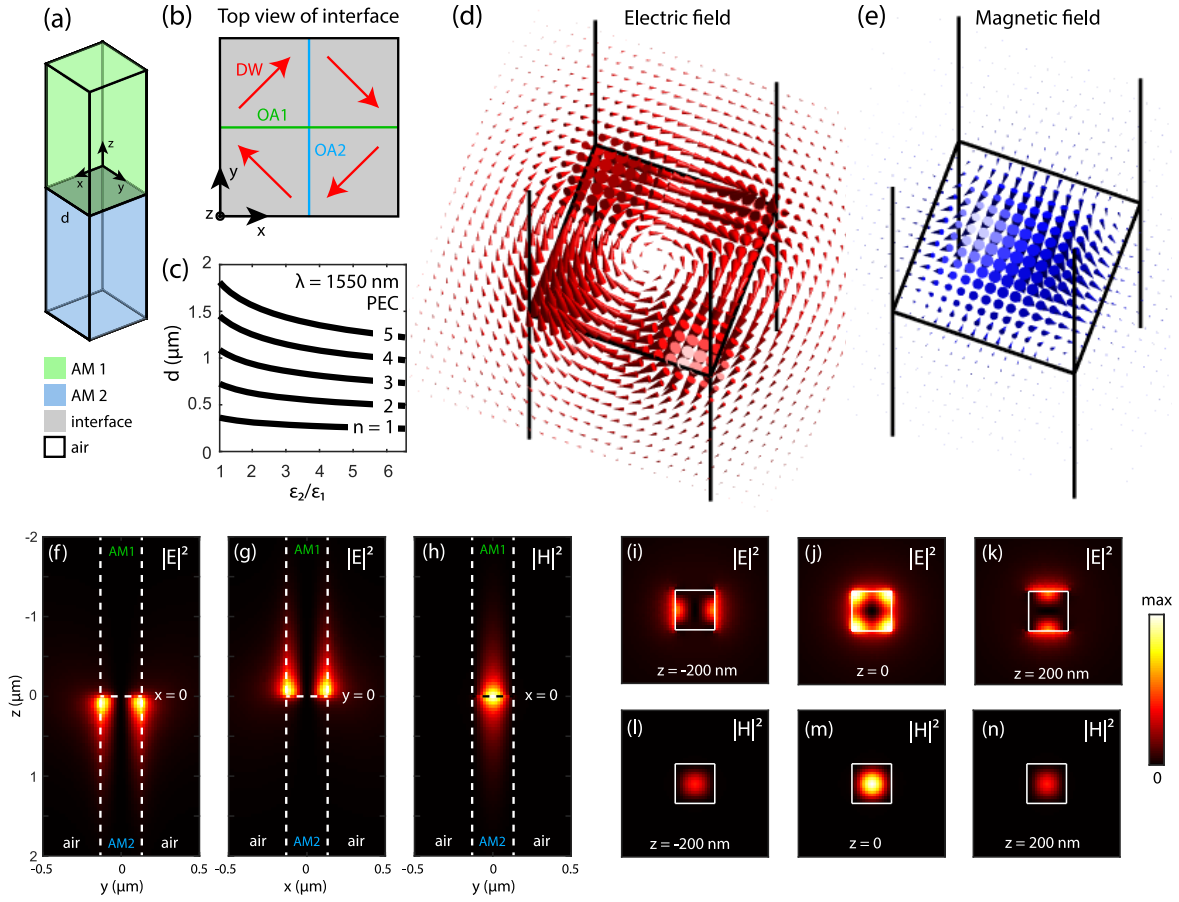

Figure 5: (a) The interface between two square cylinders made of anisotropic materials (AM). (b) The orientation of optical axes is shown by blue and green lines. Dyakonov waves reflect from the air boundaries at the angle of $\alpha = 45^\circ$ forming a two-dimensionally confined mode. (c) The anisotropy factor dependence of square widths d at which the DSCM exist for different mode orders n. (d) Electric and (e) magnetic fields calculated in the horizontal plane $z = 0$ in DSCM. Black lines denote the edges of rods. Electric (f, g, i–k) and magnetic (h, l–n) field intensities in DSCM in horizontal (i–n) and vertical (f–h) cross-sections. $d = 264.34$ nm, $\varepsilon_1 = 9$, $\varepsilon_2 = 36$, $\lambda = 1550$ nm. DSCM, Dyakonov-like surface cavity mode.

under 90° rotation about the z-axis and subsequent mirror reflection relative to the xy plane. The group theory tells us that i) S_4-symmetrical structures should have two singlet eigenmodes and one doublet eigenmode; ii) symmetries of these eigenmodes are determined by irreducible representations of the S_4 point group. To explore this in application to our system consisting of two tangent rods surrounded by air or PEC, we simulate its eigenmodes in COMSOL. Our simulations reveal that, as expected, such a system supports waveguide modes propagating along the rods, as well as DSCMs localized at the interface between the rods. We notice that the waveguide modes can be singlets or doublets while the DSCMs are always singlets. This is due to more strict selection rules for DSCM in comparison with waveguide modes. The calculated electric and magnetic field intensity profiles of the first-order DSCM in vertical and horizontal cross-sections are shown in Figure 5f–n. One can see that in the upper (or lower) rod, the electric field is mainly localized near the boundaries $y = \text{const}$ (or $x = \text{const}$), whereas at the interface between the rods ($z = 0$), it is localized near the four square's corners, thereby, having a higher degree of symmetry. In addition, at the interface, the electric vector takes the vortex shape, while the magnetic field is maximal in the center of the vortex (Figure 5d and e). Such a structure of DSCM is similar to the Mie resonances presented in Ref. [42]. Using these resonances, it is possible to obtain a strong magnetic response from a magnetic particle placed in the center of the interface. The electric and magnetic field intensity profiles in the DSCMs of the orders $n = 1$–3 are shown in Figure 6a. We notice that owing to different boundary conditions, the number of nodes (or antinodes) in electric (or magnetic) intensity field profile equals to $n \times n$ for the air boundary, and to $(n+1) \times (n+1)$ for the

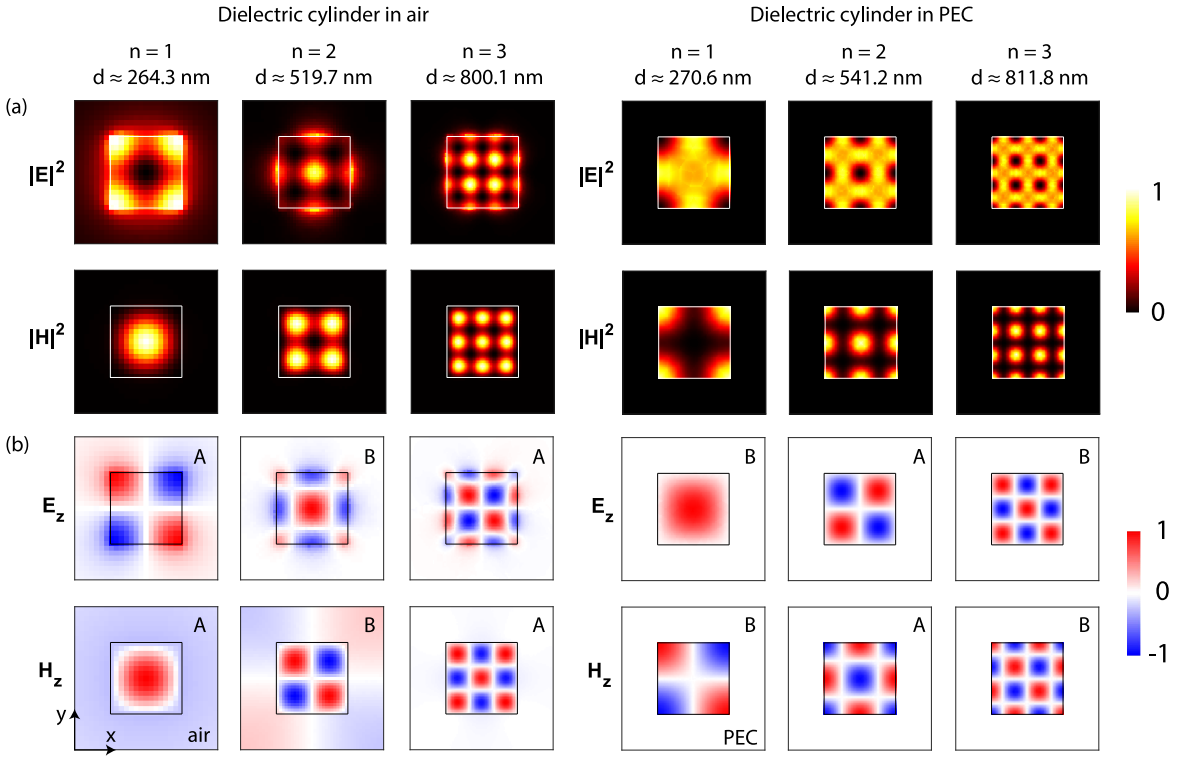

Figure 6: (Color online) Intensity (a) and *z*-projection (b) of electric and magnetic fields of DSCMs at $n = 1 - 3$ calculated for the cases of air and PEC boundaries. Symbols A or B denote irreducible representations of the S_4 point group. $\varepsilon_1 = 9$, $\varepsilon_2 = 36$, $\lambda = 1550$ nm. Colorscales are shown on the right. DSCM, Dyakonov-like surface cavity mode.

PEC boundary. To ascribe a specific irreducible representation to the obtained DSCMs, we also plot the *z*-projection of electric and magnetic vectors in Figure 6b. By inspecting Figure 6b, one can see that the displayed DSCMs refer to the irreducible representations either A or B of the S_4 point group[2].

Owing to radiation losses caused by the scattering of DSWs at the air boundaries, DSCMs should have a finite *Q*-factor when rods are surrounded by air. Generally, the *Q*-factor depends on the dielectric permittivities of rods and environment, as well as on the mode order. The COMSOL simulation reveals that for the case of air boundaries and components of dielectric tensors of rods $\varepsilon_1 = 9$ and $\varepsilon_2 = 36$, the *Q*-factor of DSCMs with $n = 1$, 2, and 3 equal to 8.83, 52.98, and 197.06, respectively. Apparently, the *Q*-factor decreases with the mode order because of increasing diffraction losses caused by the violation of the total internal reflection in smaller squares. Owing to lack of scattering and absorption losses in the rods surrounded by PEC, the corresponding *Q*-factor is infinite.

Finally, DSCMs demonstrated in this section can be generalized to the case of cylinders of arbitrary rectangular shape. A DSCM in such a structure is a superposition of DSWs reflecting from boundaries at angles α not equal to 45° and propagating at azimuthal angles φ also not equal to 45°. Such a structure is no longer S_4-symmetrical, and the corresponding field distributions are less symmetrical in comparison with the case of square cylinders (See Supplemental Materials for details). Owing to the perfect reflection from the PEC boundary (Figure 2d), the *Q*-factors of DSCMs in rectangular cylinders with PEC boundaries remain infinite.

6 Conclusion

In conclusion, we have studied Dyakonov-like surface states which appear at the interface between two identical anisotropic dielectrics twisted in such a way that their optical axes form an angle of 90° to each other. First, we have studied the case of the infinite horizontal interface where DSWs exist in a small range of azimuthal angles. In the presence of vertical boundaries that constrain the system from two sides, electromagnetic confinement

2 The difference between irreducible representations A and B in S_4 point group is whether a field changes its sign under the symmetry operation S_4. See [43] for details.

comes into play. We have demonstrated that such a one-dimensionally confined system supports DSWMs propagating along the direction where conventional DSWs do not exist. We have shown that the first-order DSWM can propagate without losses. This fact opens ample opportunities for using these modes in signal transmission lines and information processing. The existence of DSWMs can be explained in terms of the multireflection of DSWs at angles close to 45° to the interfacial strip waveguide boundaries. We have further improved this idea and considered the interface between two square cylinders made of anisotropic materials. Owing to the two-dimensional electromagnetic confinement, such a system supports Dyakonov surface cavity modes. We believe that our work can open new insights in the field of surface waves in anisotropic media, which can lead to the practical application of DSWs in optoelectronic devices.

7 Theoretical methods

To simulate the DSW reflection from a single boundary, we developed a model in COMSOL Multiphysics where the DSW is excited by a port plane. The field and the wavevector of the mode which are excited by the port are taken as a DSW solution at the infinite interface described in Section 2. Then, we find the *S*-parameters of such a system by calculating the fields at the reflection and the transmission sides. As a result, we obtain the total reflectance and transmittance of DSW at the boundary. We verified our numerical results obtained in COMSOL Multiphysics using the analytical solutions. When calculating models that do not have an analytical solution, we checked that the final results do not depend on the grid size and the position of the PML layers.

Acknowledgments: Authors acknowledge Ilia M. Fradkin for fruitful discussions.

Author contribution: All the authors have accepted responsibility for the entire content of this submitted manuscript and approved submission. D.C. conducted COMSOL simulations. E.A. developed a theoretical model, S.D. conceived the idea of this manuscript and organized the manuscript preparation, N.G. supervised the project and provided the valuable advice on the manuscript.

Research funding: This work was supported by the Russian Foundation for Basic Research (Grant No. 18-29-20032).

Conflict of interest statement: The authors declare no conflicts of interest regarding this article.

References

[1] D. L. Mills and V. M. Agranovich, "Surface Polaritons," Amsterdam, New York, Oxford; North- Holland Publishing Company: 1988.

[2] N. Malkova and C. Z. Ning, "Shockley and Tamm surface states in photonic crystals," *Phys. Rev. B*, vol. 73, no. 11, p. 113113, 2006.

[3] A. P. Vinogradov, A. V. Dorofeenko, A. M. Merzlikin, and A. A. Lisyansky, "Surface states in photonic crystals," *Phys. Usp.*, vol. 53, p. 243, 2010.

[4] S. A. Dyakov, A. Baldycheva, T. S. Perova, et al., "Surface states in the optical spectra of two-dimensional photonic crystals with various surface terminations," *Phys. Rev. B*, vol. 86, p. 115126, 2012.

[5] Y. V. Kartashov, V. A. Vysloukh, and L. Torner, "Surface gap solitons," *Phys. Rev. Lett.*, vol. 96, no. 7, p. 073901, 2006.

[6] M. I. D'yakonov, "New type of electromagnetic wave propagating at an interface," *Sov. Phys. JETP*, vol. 67, no. April, pp. 714–716, 1988.

[7] D. B. Walker, E. N. Glytsis, and T. K. Gaylord, "Surface mode at isotropic–uniaxial and isotropic–biaxial interfaces," *J. Opt. Soc. Am. A*, vol. 15, no. 1, p. 248, 1998.

[8] E. E. Narimanov, "Dyakonov waves in biaxial anisotropic crystals," *Phys. Rev.*, vol. 98, no. 1, pp. 1–13, 2018.

[9] A. Lakhtakia and J. A. Polo, "Dyakonov-Tamm wave at the planar interface of a chiral sculptured thin film and an isotropic dielectric material," *J. Eur. Opt. Soc.*, vol. 2, pp. 1–12, 2007.

[10] J. Gao, A. Lakhtakia, and M. Lei, "On dyakonov-tamm waves localized to a central twist defect in a structurally chiral material," *J. Opt. Soc. Am. B*, vol. 26, pp. B74–B82, 2009.

[11] T. Repän, O. Takayama, and A. V. Lavrinenko, "Photonics," vol. 7, 2020, p. 34.

[12] Y. Zhang, X. Wang, D. Zhang, S. Fu, S. Zhou, and X.-Z. Wang, "Unusual spin and angular momentum of dyakonov waves at the hyperbolic-material surface," *Opt. Express*, vol. 28, no. 13, pp. 19205–19217, 2020.

[13] S. Y. Karpov, "Dyakonov surface electromagnetic waves in iii-nitride heterostructures," *Phys. Status Solidi (b)*, vol. 256, no. 3, p. 1800609, 2019.

[14] I. Fedorin, "Dyakonov surface waves at the interface of nanocomposites with spherical and ellipsoidal inclusions," *Opt. Quant. Electron.*, vol. 51, no. 6, p. 201, 2019.

[15] O. Takayama, L. C. Crasovan, S. K. Johansen, D. Mihalache, D. Artigas, and L. Torner, "Dyakonov surface waves: A review," *Electromagnetics*, vol. 28, no. 3, pp. 126–145, 2008.

[16] O. Takayama, L. Crasovan, D. Artigas, and L. Torner, "Observation of dyakonov surface waves," *Phys. Rev. Lett.*, vol. 102, no. 4, pp. 2–5, 2009.

[17] O. Takayama, D. Artigas, and L. Torner, "Lossless directional guiding of light in dielectric nanosheets using Dyakonov surface waves," *Nat. Nanotechnol.*, vol. 9, no. 6, pp. 419–424, 2014.

[18] F. Chiadini, V. Fiumara, A. Scaglione, and A. Lakhtakia, "Compound guided waves that mix characteristics of surface-plasmon-polariton, Tamm, Dyakonov–Tamm, and Uller–Zenneck waves," *J. Opt. Soc. Am. B*, vol. 33, no. 6, p. 1197, 2016.

[19] A. Lakhtakia and M. Faryad, "Theory of optical sensing with Dyakonov–Tamm waves," *J. Nanophotonics*, vol. 8, p. 083072, 2014.

[20] D. P. Pulsifer, M. Faryad, and A. Lakhtakia, "Observation of the Dyakonov-Tamm wave," *Phys. Rev. Lett.*, vol. 111, no. 24, pp. 1–5, 2013.
[21] D. Artigas and L. Torner, "Dyakonov surface waves in photonic metamaterials," *Phys. Rev. Lett.*, vol. 94, no. 1, p. 013901, 2005.
[22] Z. Jacob and E. E. Narimanov, "Optical hyperspace for plasmons: dyakonov states in metamaterials," *Appl. Phys. Lett.*, vol. 93, no. 22, p. 221109, 2008.
[23] O. Takayama, D. Artigas, and L. Torner, "Practical dyakonons," *Opt. Lett.*, vol. 37, no. 20, p. 4311, 2012.
[24] O. Takayama, D. Artigas, and L. Torner, "Coupling plasmons and dyakonons," *Opt. Lett.*, vol. 37, p. 1983, 2012.
[25] T. G. Mackay, C. Zhou, and A. Lakhtakia, "Dyakonov–Voigt surface waves," *Proc. Math. Phys. Eng. Sci.*, vol. 475, p. 20190317, 2019.
[26] A. Lakhtakia and T. Mackay, "From unexceptional to doubly exceptional surface waves," *J. Opt. Soc. Am. B*, Vol. 37, no. 2, pp. 1–13, 2020.
[27] A. Lakhtakia, T. G. Mackay, and C. Zhou, "Electromagnetic surface waves at exceptional points," *Eur. J. Phys*. in press. https://doi.org/10.1088/1361-6404/abb6c7.
[28] C. Zhou, T. G. Mackay, and A. Lakhtakia, "Theory of dyakonov–tamm surface waves featuring dyakonov–tamm–voigt surface waves," *Optik*, Vol. 211, p. 164575, 2020.
[29] V. Kajorndejnukul, D. Artigas, and L. Torner, "Conformal transformation of Dyakonov surface waves into bound states of cylindrical metamaterials," *Phys. Rev. B*, vol. 100, no. 19, pp. 1–6, 2019.
[30] K. Y. Golenitskii, A. A. Bogdanov, "Dyakonov-like surface waves in anisotropic cylindrical waveguides," *Phys. Rev. B*, vol. 110, no. 16, p. 165434, 2020.
[31] N. Averkiev and M. Dyakonov, "Electromagnetic waves localized at the boundary of transparent anisotropic media," *Opt. Spectrosc.*, vol. 68, no. 5, pp. 1118–1121, 1990.
[32] A. N. Darinskii, "Dispersionless polaritons on a twist boundary in optically uniaxial crystals," *Crystallogr. Rep.*, vol. 46, no. 5, pp. 842–844, 2001.
[33] A. N. Furs, V. M. Galynsky, and L. M. Barkovsky, "Dispersionless surface polaritons at twist boundaries of crystals and in a transition layer between the crystals," *Opt. Spectrosc.*, vol. 98, no. 3, pp. 454–461, 2005.
[34] A. N. Furs, V. M. Galynsky, and L. M. Barkovsky, "Surface polaritons in symmetry planes of biaxial crystals," *J. Phys. Math. Gen.*, vol. 38, pp. 8083–8101, 2005.
[35] S. R. Nelatury, J. A. Polo Jr., and A. Lakhtakia, "Surface waves with simple exponential transverse decay at a biaxial bicrystalline interface," *J. Opt. Soc. Am. A*, vol. 24, p. 856, 2007.
[36] J. A. Polo Jr., S. R. Nelatury, and A. Lakhtakia, "Surface waves at a biaxial bicrystalline interface," *J. Opt. Soc. Am. A*, vol. 24, no. 9, p. 2974, 2007.
[37] V. I. Alshits and V. N. Lyubimov, "Dispersionless surface polaritons in the vicinity of different sections of optically uniaxial crystals," *Phys. Solid State*, vol. 44, no. 2, pp. 386–390, 2002.
[38] O. Takayama, A. Y. Nikitin, L. Martin-Moreno, L. Torner, and D. Artigas, "Dyakonov surface wave resonant transmission," *Opt. Express*, vol. 19, no. 7, p. 6339, 2011.
[39] L. Li, "Fourier modal method for crossed anisotropic gratings with arbitrary permittivity and permeability tensors," *J. Opt. Pure Appl. Opt.*, vol. 5, no. 4, p. 345, 2003.
[40] T. Weiss, G. Granet, N. A. Gippius, S. G. Tikhodeev, and H. Giessen, "Matched coordinates and adaptive spatial resolution in the fourier modal method," *Opt. Express*, vol. 17, no. 10, pp. 8051–8061, 2009.
[41] S. G. Tikhodeev, A. L. Yablonskii, E. A. Muljarov, N. A. Gippius, and T. Ishihara, "Quasiguided modes and optical properties of photonic crystal slabs," *Phys. Rev. B*, vol. 66, p. 045102, 2002.
[42] A. García-Etxarri, R. Gómez-Medina, L. S. Froufe-Pérez, et al., "Strong magnetic response of submicron Silicon particles in the infrared," *Opt. Express*, vol. 19, p. 4815, 2011.
[43] http://symmetry.jacobs-university.de.
[44] E. V. Anikin, D. A. Chermoshentsev, S. A. Dyakov, N. A. Gippius, "Dyakonov-like waveguide modes in an interfacial strip waveguide," *Phys. Rev. B*, vol. 102, no. 16, p. 161113(R), 2020.

Supplementary Material: The online version of this article offers supplementary material (https://doi.org/10.1515/nanoph-2020-0459).